ARTICLE NO. 79-4144

Boundary-Layer Charged-Particle Density Profiles in an Atmospheric Pressure Plasma Flow

M. Suzuki* and A. Kanzawa†
Tokyo Institute of Technology, Tokyo, Japan

The charged-particle density profiles inside the boundary layer formed on a flat plate or a circular cylinder located in an atmospheric pressure plasma flow were measured with electrostatic probes. Theoretical profiles were obtained through numerical solution of momentum, species, and energy conservation equations taking account of variable transport properties. Comparison of these results leads to the following conclusions: For the flat plate boundary layer, the measured charged-particle density at the bottom of the boundary layer is higher than that calculated for the thermochemical equilibrium condition and is close to the result calculated based on "frozen" chemistry; but the state in other parts of the boundary layer deviates from the "frozen" chemistry condition. For the cylindrical boundary layer, the measured charged-particle density is near the "frozen" state in the neighborhood of the stagnation point, but it approaches the thermochemical equilibrium state as the angle from the stagnation point increases. Furthermore, it was found that the state in the cylindrical boundary layer changes fairly abruptly from "frozen" to "thermochemical equilibrium" at the angle of 110 deg ~ 120 deg, which is in the neighborhood of the separation point.

Nomenclature

A = area of probe electrode surface
a = probe surface width
C = $\rho\mu/\rho_0\mu_0$
c_p = specific heat at constant pressure
c_p^* = c_p/c_{p0}
c_j = mass fraction of j particle
D = ambipolar diffusion coefficient
d = thickness of electrical sheath
E = $\pi e^{\pi\lambda}$
E_i = ionization energy
$-e$ = charge of electron
$F(\phi)$ = function defined by Eq. (18)
f' = u/u_0
g = H_t/H_{t0}
H_t = total enthalpy
H = enthalpy
h_t = heat-transfer coefficient
I = probe current
K_i = mobility of ion
k = Boltzmann's constant
Le = Lewis number
m_j = mass of j particle
Nu_x = Nusselt number $(h_t x/\kappa)$
Nu_d = Nusselt number $(h_t d/\kappa)$
n_j = number density of j particle
Pr = Prandtl number
Re_x = Reynolds number (ux/ν)
Re_d = Reynolds number (ud/ν)
r = radial coordinate
r_p = probe radius
r_0 = cylinder radius
Sc = Schmidt number
T = temperature
t^* = nondimensional temperature $(T-T_w)/(T_0-T_w)$
t_1 = nondimensional temperature $T/(T_0-T_w)$
u = velocity of x direction
u_0 = velocity of external flow
u_r = velocity of r direction
u_θ = velocity of θ direction
V = absolute value of probe potential
v = velocity of y direction
v_d = diffusion velocity
v_g = gas phase reaction velocity
$\bar{v}$ = mean velocity of particles
w_j = production rate of j component
x = distance from flat plate edge
y = distance from flat plate wall
z = c_i/c_{i0}
α = recombination coefficient
δ = thickness of boundary layer
ϵ = $5/2\,(RT/E_i)$
ζ = Damköhler number
λ = quantity defined by Eq. (9)
η = $u_0/(2\xi)^{1/2}\int_0^y \rho dy$
θ = angle from stagnation point
κ = thermal conductivity
κ^* = κ/κ_0
μ = viscosity
μ^* = μ/μ_0
ν = kinematic viscosity
ξ = $\int_0^x \rho_0\mu_0 u_0 dx$
ρ = density
ρ^* = ρ/ρ_0
$(\rho D)^*$ = $\rho D/\rho_0 D_0$
σ = quantity defined by Eq. (9)
τ_d = diffusion time
τ_g = reaction time of gas phase
ϕ = probe angle against flow direction
χ = eV/kT
ψ = stream function
ψ^* = nondimensional stream function
ω = vorticity
ω^* = nondimensional vorticity $w/(u_0/r_0)$

Subscripts

a = atom
e = electron
h = heavy particles (ion and atom)

Received Jan. 3, 1979; revision received April 23, 1979.

Index categories: Boundary Layers and Convective Heat Transfer—Laminar; Plasma Dynamics and MHD; Reactive Flows.

*Research Associate, Research Laboratory for Nuclear Reactors.
†Associate Professor, Dept. of Chemical Engineering.

i = ion
j = j particle
w = wall
0 = boundary-layer edge
$\perp$ = perpendicular to flow
$\parallel$ = parallel to flow

I. Introduction

FOR the problem concerning transport phenomena, e.g., heat transfer between a plasma flow and a solid wall, which has appeared in many practical situations, it is important to know the state inside the boundary layer near the solid wall. In particular, thermal plasma flow at atmospheric pressure is often used as a source of heat in plasma furnaces, etc., so it is necessary to investigate the state of the boundary layer in this condition. The state inside the boundary layer changes between "frozen" and "thermochemical equilibrium" by a balance between the diffusion time of charged particles (ions and electrons) across the boundary layer and the gas phase recombination time.

Several theoretical analyses[1-4] of the ionized boundary-layer flow have been carried out, with the objective of obtaining the current-voltage characteristics of the electrode on the solid surface where the plasma sheath was either collision dominated or collision free. Experimental data are relatively scarce. There are only a few reports concerning the flat plate boundary layer at low pressure,[5,6] and they show that the state inside the boundary layer is near "frozen." However, this condition does not always hold at higher pressures, because at high pressures the collision of particles in the boundary layer occurs more frequently than at low pressures.

In this study, an atmospheric pressure argon plasma jet with known temperature and velocity distributions was used as a plasma flow source. The charged-particle densities inside the boundary layer formed on the flat plate or the circular cylinder located in the flow were measured with electrostatic probes. Theoretical profiles were obtained through numerical solution of momentum, species, and energy conservation equations taking account of variable transport properties. By comparing experimental and theoretical results, the states of the boundary layers were investigated about the y direction for the flat plate and about the θ direction for the circular cylinder.

II. Experimental Apparatus and Method

Experiments reported here were performed using the plasma jet produced by the arc discharge between an anode (copper nozzle) and a cathode (tungsten rod). A detailed description of the equipment has been given elsewhere.[7] The temperature and velocity distributions of the plasma jet, which are shown in Fig. 1, also have been obtained by the method described in the same report. And, it is confirmed that the state inside the plasma jet is at thermochemical equilibrium.

The electrostatic probe for measuring charged-particle densities was made of 0.2-mm-diam platinum wire covered by a porcelain tube (0.2 mm i.d., 0.5 mm o.d.), whose end was flattened so as to be used as the electrode surface as shown in Fig. 2. The flat plate used was made of brass with a square base (8 × 8 mm) as shown in Fig. 4A. The cylinder used was a stainless steel (or copper) tube with a diameter of 2 mm. The probe can be traversed with an accuracy of 0.1 mm in the x and y directions by the adjuster. As shown in Fig. 3, both the flat plate (or cylinder) and the probe were attached to a turntable whose rotating velocity was variable. After the probe was set to pass through a certain position in the plasma jet, it was swept with a velocity of 0.86 m/s through the plasma flow by the turntable; this was done to avoid thermal damage to the probe.

The experiments for the flat plate were performed for three-way directions of the probe to the flat plate (Figs. 4A, a-c)

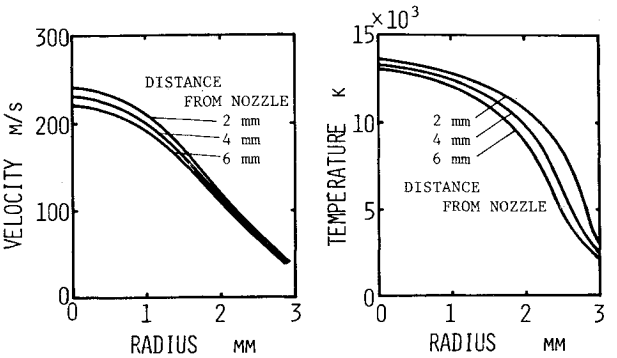

Fig. 1 Velocity and temperature distributions of plasma jet.

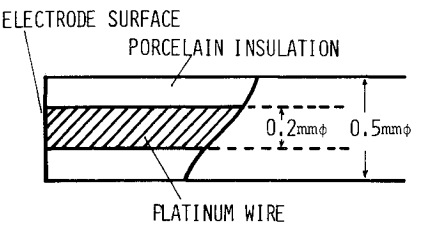

Fig. 2 Cross-sectional view of probe.

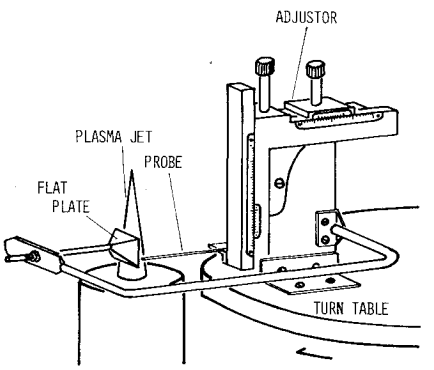

Fig. 3 Outline of the experimental apparatus.

considering the influence of the flow direction on the probe current. The charged-particle density in the neighborhood of the flat plate wall was measured with the probe imbedded in the flat plate and flattened (flush probe) as shown in Fig. 4A, d. The experiments for the cylinder were also done with the probe located as shown in Fig. 4B. In these experiments, the position of the edge of the flat plate or the stagnation point of the cylinder was always at the section, 2 mm from the nozzle exit of a plasma jet.

The charged-particle densities inside the boundary layers could be obtained by measuring the ion-saturated current that flows into the negatively biased probe, because it was dominated by ambipolar diffusion ions and electrons. In this experiment, the ion current was saturated in the range of $V < -10$ V, so the constant probe potential of -12 V was used.

The obtained ion saturated current distribution in the flat plate boundary layer at $x = 2$ mm is shown in Fig. 5 as an example. Similar distributions were obtained at $x = 1$ and 4 mm. For the cylindrical boundary-layer measurement, the similar experiments were performed with those probes with the probe in the direction of the plasma flow as shown in Fig. 4B. Flush probes were imbedded at $x = 1,2$, and 4 mm in the center of the flat plate. Data for these probes were obtained at probe potentials of -10, -20, and -30 V and at $x = 2$ mm. Ion currents of 3.6×10^{-4}, 4.4×10^{-4}, and 4.8×10^{-4} A were obtained for each probe potential. For the measurement

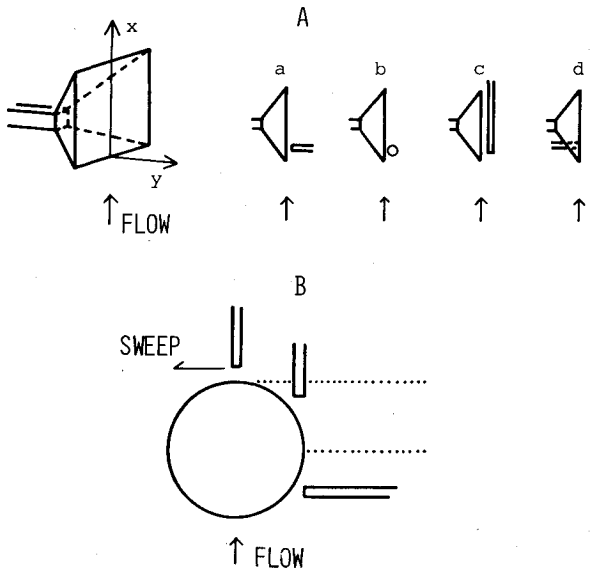

Fig. 4 Flow direction and probe directions.

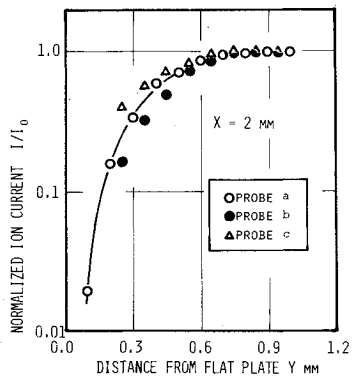

Fig. 5 Measured ion current distribution in the flat plate boundary layer.

in the rear flow of the cylinder, the water-cooled copper tube located in the plasma flow was used, and only the probe was swept perpendicularly to the tube axis, so that continuous data could be obtained in this region.

III. Numerical Analysis

In order to compare experimental profiles with theoretical ones, a numerical analysis of each conservation equation of hydrodynamics was carried out assuming "frozen" or "thermochemical equilibrium." The properties of argon required in this analysis were ρ, μ, κ, D, and c_p, which change abruptly at the temperature around 10,000 K where ionization reaction mainly occurs. Therefore, for the plasma flow of 13,240 K used in the present experiments, this influence must be considered when these equations are solved. In this study, the plasma was considered to be a mixture consisting of atoms, ions, and electrons, and its properties were obtained using the simple kinetic theory.[8]

The present calculations contain the following assumptions which are satisfied in our experiments: 1) steady flow; 2) two-dimensional flow; 3) an ambipolar diffusion process; 4) a very thin electrical sheath, so that this effect is not considered; 5) no applied external electric and magnetic fields; 6) plasma consisting of atoms, ions (singly ionized), and electrons with the same temperature. Under these assumptions, for both the flat plate boundary layer and cylindrical one, the numerical analyses were carried out.

A. Flat Plate Boundary Layer

For the flat plate boundary layer, a numerical analysis was carried out for the cases of "frozen" and "thermochemical equilibrium." For the fields of flow, temperature and charged-particle density, the laminar flat plate boundary-layer equations for the similarity solution are given by Back[9] as follows:

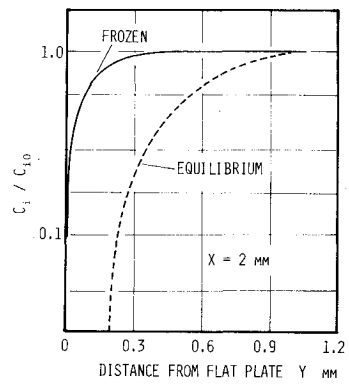

Fig. 6 Result of numerical calculation for the flat plate boundary layer.

$$(Cf'')' + ff'' = 0 \tag{1}$$

$$\left[\frac{C}{Pr}g' + \frac{C}{Pr}(Le-1)\left(\frac{c_{i0}E_i}{H_{t0}}\right)(1+\epsilon)z'\right] + fg' + \frac{u_0^2}{2H_{t0}}\left[2C\left(1-\frac{1}{Pr}\right)f'f''\right] = 0 \tag{2}$$

$$\left(C\frac{Le}{Pr}z'\right)' + fz' + \frac{2}{u_0 c_{i0}\mathrm{d}\xi/\mathrm{d}x}\left(\frac{wi}{\rho}\right) = 0 \tag{3}$$

where the boundary conditions are $\eta = 0$: $f(0) = 0$, $g(0) = g_w$, $z(0) = z_w$. $\eta \to \infty$: $f'(\eta) \to 1$, $g(\eta) \to 1$, $z(\eta) \to 1$.

Numerical solutions of Eqs. (1-3) were carried out by a Runge-Kutta-Gill method using the properties calculated at each position of the boundary layer. The boundary conditions are $T_0 = 13{,}240$ K, $u_0 = 230$ m/s, $c_{i0} = 0.26$ (the values of thermochemical equilibrium state at 13,240 K), $T_w = 500$ K, and $z_w = 0$. In the "frozen" case, numerical solutions could be obtained by integration of Eqs. (1-3) using the aforementioned method. But in the case of "thermochemical equilibrium," it is impossible to obtain the solutions of Eqs. (1-3) analytically, so Saha's equation was taken instead of Eq. (3) and the solution was obtained by the similar method. Figure 6 shows the results obtained. The solid and broken lines indicate the "frozen" and "thermochemical equilibrium" cases, respectively.

B. Cylindrical Boundary Layer

For the cylindrical boundary layer, the boundary-layer approximation cannot be used. Here, in order to simplify the equations, the assumptions that the kinetic energy is neglected and the dissipation term is neglected (about 1%) were added. Under these assumptions, a numerical analysis was carried out for two cases of "frozen" and "thermochemical equilibrium."

For the basic equations in the two-dimensional cylindrical coordinate (r, θ), the following stream function and vorticity

$$u_r = -\frac{1}{\rho r}\frac{\partial \psi}{\partial \theta}, \quad u_\theta = \frac{1}{\rho}\frac{\partial \psi}{\partial r} \tag{4}$$

$$\omega = \frac{u_\theta}{r} + \frac{\partial u_\theta}{\partial r} - \frac{1}{r}\frac{\partial u_r}{\partial \theta} \tag{5}$$

were introduced and transformed with the coordinate λ, σ (Ref. 10):

$$r = r_0 \exp(\pi\lambda) \qquad \theta = \pi\sigma \tag{6}$$

Each variable was nondimensionalized as follows:

$$\psi^* = \frac{\psi}{\rho_0 \mu_0 r_0}, \quad \omega^* = \frac{\omega}{u_0/r_0}, \quad t^* = \frac{T-T_w}{T_0-T_w}, \quad t_l = \frac{T}{T_0-T_w}$$

$$Re = \frac{\rho_0 \mu_0 d_0}{\mu_0}, \quad Pr = \frac{c_{p0}\mu_0}{\kappa_0}, \quad Sc = \frac{\mu_0}{\rho_0 D_0}, \quad \kappa^* = \frac{\kappa}{\kappa_0}$$

As a result, the following equations to be solved were obtained:

$$\frac{\partial\psi^*}{\partial\lambda}\cdot\frac{\partial\omega^*}{\partial\sigma} - \frac{\partial\psi^*}{\partial\sigma}\cdot\frac{\partial\omega^*}{\partial\lambda} - \frac{2}{Re}\mu^*\left(\frac{\partial^2\omega^*}{\partial\lambda^2}+\frac{\partial^2\omega^*}{\partial\sigma^2}\right) = [\mu,\rho] \quad (7)$$

$$\omega^* - \frac{1}{\rho^*}\cdot\frac{1}{E^2}\left(\frac{\partial^2\psi^*}{\partial\lambda^2}+\frac{\partial^2\psi^*}{\partial\sigma^2}\right) = [\rho] \quad (8)$$

$$\frac{\partial\psi^*}{\partial\lambda}\cdot\frac{\partial c_i}{\partial\sigma} - \frac{\partial\psi^*}{\partial\sigma}\cdot\frac{\partial c_i}{\partial\lambda} = \frac{2}{Re}\cdot\frac{1}{Sc}\left[(\rho D)^*\left(\frac{\partial^2 c_i}{\partial\lambda^2}+\frac{\partial^2 c_i}{\partial\sigma^2}\right) + \frac{\partial\{(\rho D)^*\}}{\partial\lambda}\cdot\frac{\partial c_i}{\partial\lambda} + \frac{\partial\{(\rho D)^*\}}{\partial\sigma}\cdot\frac{\partial c_i}{\partial\sigma}\right] + E^2\frac{r_0 w_i}{\rho_0\mu_0} \quad (9)$$

$$\frac{\partial\psi^*}{\partial\lambda}\left(\frac{\partial t}{\partial\sigma}+\frac{t_l}{1+c_i}\cdot\frac{\partial c_i}{\partial\sigma}\right) - \frac{\partial\psi^*}{\partial\sigma}\left(\frac{\partial t}{\partial\lambda}+\frac{t_l}{1+c_i}\cdot\frac{\partial c_i}{\partial\lambda}\right) = \frac{2}{Re}\cdot\frac{1}{Pr}\cdot\frac{1}{c_p^*}\left[\kappa^*\left(\frac{\partial^2 t}{\partial\lambda^2}+\frac{\partial^2 t}{\partial\sigma^2}\right)+\frac{\partial\kappa^*}{\partial\lambda}\cdot\frac{\partial t}{\partial\lambda}+\frac{\partial\kappa^*}{\partial\sigma}\cdot\frac{\partial t}{\partial\sigma}\right] + \frac{1}{1+c_i}\left[\frac{2}{Re}\cdot\frac{1}{Sc}\left\{(\rho D)^* t_l\left(\frac{\partial^2 c_i}{\partial\lambda^2}+\frac{\partial^2 c_i}{\partial\sigma^2}\right) + \frac{\partial\{(\rho D)^* t_l\}}{\partial\lambda}\cdot\frac{\partial c_i}{\partial\lambda} + \frac{\partial\{(\rho D)^* t_l\}}{\partial\sigma}\cdot\frac{\partial c_i}{\partial\sigma}\right\}\right] \quad (10)$$

Here, $[\mu,\rho]$ and $[\rho]$ show the term consisting of the differential terms of μ and ρ, so that they are zero when μ and ρ are constant. Equations (7-10) are transformed into the difference equations, and the numerical calculation is carried out taking into account the variation of properties in the boundary layer. But it is difficult to calculate those equations directly, so the following method was used: 1) In the flowfield, a numerical calculation was carried out assuming that properties are constant: $[\mu,\rho] = 0$, $[\rho] = 0$, μ^*, and $\rho^* = 1$. In this case, a Reynolds number of 46.2, which is equivalent to the outer flow, was taken as a typical property. 2) Using the preceding result of the flowfield, the two solutions assuming the frozen state [$w_i = 0$ in Eq. (9)] and the thermochemical equilibrium [using Saha's equation instead of Eq. (9)] were calculated. The obtained results are shown in Fig. 7 as the isodensity lines of charged-particles.

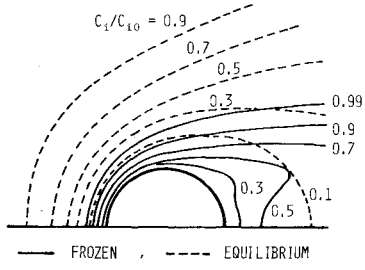

Fig. 7 Result of numerical calculation for the cylindrical boundary layer.

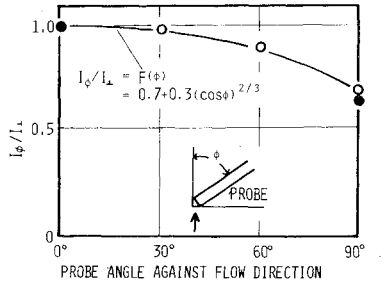

Fig. 8 Effect of probe angle on ion current.

IV. Methods of Data Reduction

For the probe imbedded into the flat plate placed parallel to a plasma flow, the equation that combines the ion current with the charged-particle density has been obtained by Clements[11] using the analogy between the heat and mass transfer for a case similar to our experimental conditions. We also used the same method to evaluate the charged-particle density from the ion current.

In this experiment the probe surface was considered to be the flat plate. When the electrode surface of the probe was placed parallel to a plasma flow, the heat-transfer equation for the flat plate parallel to a flow was used; when it was placed perpendicular to a plasma flow, the equation of a perpendicular one was used. For the parallel flat plate, the local Nusselt number has been given by[12]

$$Nu_x = 0.332\cdot Re_x^{1/2}\cdot Pr^{1/3} \quad (11)$$

where x is the distance from the edge of the flat plate. For the perpendicular one, the following,[13]

$$Nu_x = 0.572\cdot Re^{1/2}\cdot Pr^{2/5} \quad (12)$$

has been given, where x is the distance from the center of the stagnation point. Since the velocity of the front surface of this flat plate is given by $u/u_0 = 0.78\ [x/(d/2)]$, the heat-transfer coefficient of Eq. (12) is independent of x. So, using the analogy between heat and mass transfer, the following equations can be obtained. In the case that the probe surface is placed parallel to a plasma flow,

$$I_\parallel = 0.332\cdot Sc^{1/3}\cdot Re_x^{1/2}\cdot(D/x)c_i eA \quad (13)$$

In the perpendicular case,

$$I_\perp = 0.771\cdot Sc^{2/5}\cdot Re_d^{1/2}\cdot(D/d)c_i eA \quad (14)$$

By using these equations, the charged-particle density at each position could be estimated from the measured ion current. To substantiate the availability of the preceding equations, the ion current in the main stream of a plasma jet was measured with the probe that was placed parallel or perpendicular to the plasma flow, and the charged-particle density was calculated. The values measured by two different methods were $n_i = 1.21 \times 10^{17}$ cm^{-3} [using Eq. (13)] and $n_i = 1.25 \times 10^{17}$ cm^{-3} [using Eq. (14)], respectively. These values almost agreed with the value $n_i = 1.17 \times 10^{17}$ cm^{-3} in the thermochemical equilibrium state at 13,240 K within experimental error.

In the cylindrical boundary layer, particularly, the electrode of a probe faces the various flow directions; hence, this effect was investigated. At a fixed position of plasma flow, the ion-saturated current was measured changing the direction of the probe electrode to a flow. This experimental result is shown by open circles in Fig. 8. Here, ϕ is the angle of the probe to a flow, and solid circles show the theoretical value obtained by Eqs. (13) and (14) for an equal value of c_i. It is shown that this almost agrees with the experimental value. From this result, when the electrode surface was not placed parallel or perpendicular to a flow, the correction factor

$$F(\phi) = (I_\phi/I_\perp) = 0.7+0.3(\cos\phi)^{2/3} \quad (15)$$

was used and the charged-particle density at various points could be calculated using Eqs. (14) and (15).

In these calculations, values of properties ρ, μ, and D and flow velocity were required; hence, the values obtained in the "frozen" numerical solution were used. Although the choice of these values was a problem, it was verified that the result made no great difference from that using the values obtained in the "thermochemical equilibrium" numerical solution.

The data obtained by the flush probe, which was imbedded into a flat plate in order to investigate charged-particle density in its neighborhood, were analyzed by the following method. For the sheath (its thickness was very thin) that was formed on the electrode surface, the equation (of space-charged limited current)

$$\frac{I}{A} = \frac{9}{32}\frac{K_i}{\pi}\frac{V^2}{d^3} \tag{16}$$

was applied. Substituting the measured V and I and the calculated value of mobility of ions (K_i), the sheath thickness d is obtained. Using this value and the result of the aforementioned numerical solution, the charged-particle density (n_i) at the distance from the wall (d) can be obtained for each value of "frozen" and "thermochemical equilibrium." Which value should be used may be determined by whether

$$\frac{I}{A} = \frac{1}{4} n_i e \bar{v} \tag{17}$$

is satisfied or not. In this case, it was found that the solution for "frozen" satisfied this condition, and using this solution the charged-particle density (n_i) at (d) was obtained.

V. Results and Discussions

A. Flat Plate Boundary Layer

The obtained experimental and theoretical results are shown in Fig. 9 as the ratio of the degree of ionization to that in the outer flow. From this figure, it is found that in the present condition the state inside the flat plate boundary layer is not necessarily "frozen" and a certain degree of recombination of ions and electrons occurs there, although the state of the neighborhood of the wall is close to "frozen."

In order to support experimentally the assumption that the similarity solution holds in the boundary layer, the charged-particle density profiles measured at $x=1,2$, and 4 mm were plotted together with η, using properties obtained theoretically, as shown in Fig. 10. This figure, in which the data are on an identical curve, supports the assumption roughly.

These experiments were performed under the condition that the flat plate is at the floating potential, so it is necessary to consider this influence. A voltage of $-24 \sim +6$V was given to the flat plate from the anode of the plasma jet, and the charged-particle density profiles and the potential distributions inside the boundary layer were measured by the similar method. As a result, it was found that the profiles almost agreed with those at the floating potential and the potential gradient was very small in the region of $x > 0.1$ mm, so that the influence of the potential on those was considered to be negligible. This is caused by the fact that, for the negative potential, a drop occurs in the sheath whose thickness is very thin; and, for the positive potential, the potential varies gently in the entire region of the boundary layer.

The assumption that the electron temperature is equal to that of heavy particles may be justified by the following calculation and the reference in which the probe characteristics in an atmospheric pressure argon plasma were investigated experimentally and theoretically.[14] The diffusion and collision times of electrons in the boundary layer could be estimated using the following equations, respectively.

$$\tau_d = \frac{\delta/2}{v_d} = \frac{\delta}{2}\Big/\left(\frac{D_e}{n_e}\frac{dn_e}{dx}\right) \sim \frac{\delta^2}{8D_e} \tag{18}$$

$$\tau_c = v_e \lambda_e \tag{19}$$

Using these values, the number of collisions of electrons in the boundary layer was found to have a large value (about 10^9).

B. Cylindrical Boundary Layer

Figure 11 shows the isodensity lines of charged particles obtained by experiments. From the comparison with the theoretical results of Fig. 7 it is found that it is close to the result of "frozen" in the neighborhood of the stagnation point, but it has a tendency to extend outward at an angle of attack of about 120 deg. In Fig. 12, the charged-particle density profiles at $\theta=90$ deg and $\theta=132$ deg obtained by experiments are shown with the theoretical profiles of the "frozen" state. This figure shows that at $\theta=90$ deg the experimental profile agrees approximately with the theoretical one, but at $\theta=132$ deg it deviates from that. In order to make this tendency clear, the charged-particle density at the position of the half-thickness of the boundary layer was plotted as shown in Fig. 13. From this figure, in which the theoretical "frozen" and "thermochemical equilibrium" profiles were illustrated together, it is found that the state in the boundary layer changes fairly abruptly from "frozen" to "thermochemical equilibrium" at an angle of 110 ~ 120 deg.

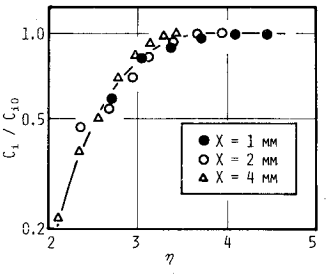

Fig. 10 Similarity of the flat plate boundary layer.

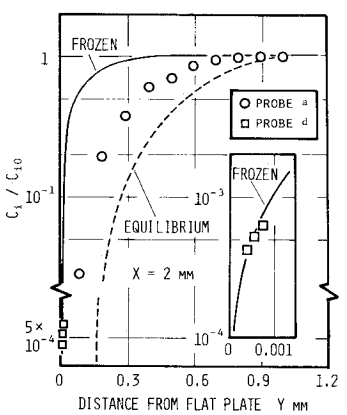

Fig. 9 Experimental and theoretical results for the flat plate boundary layer.

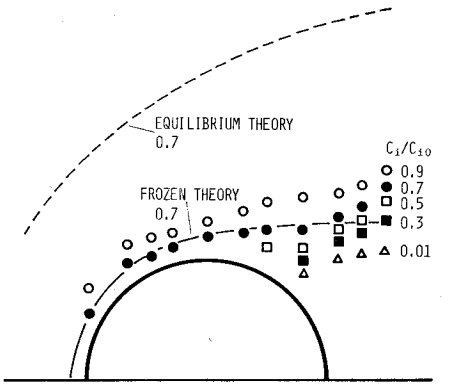

Fig. 11 Experimental result for the cylindrical boundary layer.

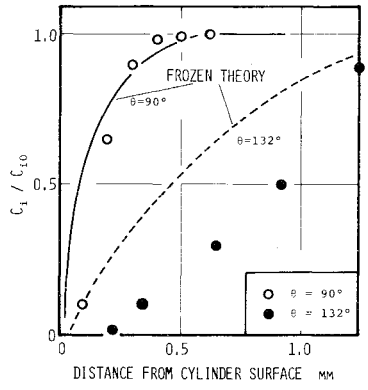

Fig. 12 Charged-particle density vs distance from cylinder wall at different angle from stagnation point.

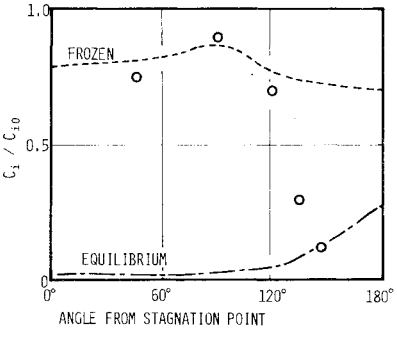

Fig. 13 Charged-particle density at half-thickness of frozen state boundary layer obtained by numerical solution.

From these results, it was confirmed that the state of the boundary layer is close to "frozen" in the region of $\theta < 110$ deg and is close to "thermochemical equilibrium" in the region of $\theta > 120$ deg. This is considered to be caused mainly by the growth of the thickness of the boundary layer as θ increases. The Damköhlar number, by which the state in the boundary layer can be decided to be "frozen" or "thermochemical equilibrium," is shown by the following forms[15]:

$$\zeta = \frac{\tau_d}{\tau_g} \sim \frac{\delta / v_d}{v_g} \sim \frac{\alpha n_i \delta^2}{D} \tag{20}$$

It indicates "frozen" for $\zeta \ll 1$ and "thermochemical equilibrium' for $\zeta \gg 1$. Since this number is proportional to the square of the thickness of the boundary layer (δ), it is found that the value of δ strongly influences ζ. In addition to this fact, considering that its abrupt change occurs in the neighborhood of the separation point of $\theta = 110$ deg $\sim$ 120 deg, it may be guessed that the turbulent flow induced by the separation has the influence on the gas phase reaction. The degree of the gas phase recombination reaction is given by the recombination coefficient α, but it is difficult to treat it quantitatively in the present situation because the recombination coefficient depends significantly on its mechanism, conditions and the effect of the turbulent flow which are unknown.

VI. Conclusions

From the foregoing studies for the atmospheric pressure plasma the following conclusions have been obtained.

For the flat plate boundary layer, it was shown that in the atmospheric pressure the measured charged-particle density at the bottom of the boundary layer is higher than that calculated for the thermochemical equilibrium condition and is close to the result calculated based on "frozen" chemistry; but the state in other parts of the boundary layer deviates from the "frozen" chemistry condition, although the boundary layer in the low pressure is "frozen" for the entire range.

For the cylindrical boundary layer, it was shown in the present condition that the charged particle density of it is near the frozen state in the neighborhood of the stagnation point, but it approaches the thermochemical equilibrium as the angle from the stagnation point increases. Furthermore, it was found that the state in the boundary layer changes fairly abruptly from "frozen" to "thermochemical equilibrium" at the angle of 110 deg $\sim$ 120 deg, which is in the neighborhood of the separation point.

References

[1] Chung, P.M. and Blankenship, V.D., "Theory of Electrostatic Double Probe Comprised of Two Parallel Plates," *AIAA Journal*, Vol. 4, March 1966, pp. 442-450.

[2] Lam, S.H., "A General Theory for the Flow of Weakly Ionized Gases," *AIAA Journal*, Vol. 2, Feb. 1964, pp. 256-262.

[3] Su, C.H., "Compressible Plasma Flow over a Biased Body," *AIAA Journal*, Vol. 3, May 1965, pp. 842-848.

[4] Talbot, L., "Theory of the Stagnation-Point Langmuir Probe," *The Physics of Fluids*, Vol. 3, Feb. 1960, pp. 289-298.

[5] Tseng, R.C. and Talbot, L., "Flat Plate Boundary-Layer Studies in a Partially Ionized Gas," *AIAA Journal*, Vol. 9, July 1971, pp. 1365-1372.

[6] Bredfeldt, H.R., Scharfman, W.E., Guthart, H., and Morita, T., "Boundary-Layer Ion Density Profiles as Measured by Electrostatic Probes," *AIAA Journal*, Vol. 5, Jan. 1967, pp. 91-98.

[7] Kanzawa, A. and Kimura, I., "Measurements of Viscosity and Thermal Conductivity of Partially Ionized Argon Plasmas," *AIAA Journal*, Vol. 5, July 1967, pp. 1315-1319.

[8] Kimura, I. and Kanzawa, A., "Experiments on Heat Transfer to Wires in a Partially Ionized Argon Plasma," *AIAA Journal*, Vol. 3, March 1965, pp. 476-481.

[9] Back, L.H., "Laminar Boundary-Layer Heat Transfer from a Partially Ionized Monatonic Gas," *The Physics of Fluids*, Vol. 10, April 1967, pp. 807-819.

[10] Son, J.S. and Hanratty, T.J., "Numerical Solution for the Flow Around a Cylinder at Reynolds Numbers of 40, 200 and 500," *Journal of Fluid Mechanics*, Vol. 35, Feb. 1969, pp. 369-386.

[11] Clements, R.M. and Smy, P.R., "Sheath-Convection Effects with Flush-Mounted Electrostatic Probes," *Canadian Journal of Physics*, Vol. 49, Oct. 1971, pp. 2540-2546.

[12] Schlichting, H., *Boundary-Layer Theory*, 6th ed., McGraw-Hill, New York, 1968, p. 285.

[13] *Dennetsu Kogaku Shiryo*, 3rd ed., Japan Society of Mechanical Engineers, Tokyo, 1975, p. 35.

[14] Kimura, I. and Negishi, N., "A Study on Probe Measurements of Flowing Partially-Ionized High-Density Gases," *Journal of the Faculty of Engineering, Univ. of Tokyo (B)*, Vol. 29, 1968, pp. 261-278.

[15] Chung, P.M., "Chemically Reacting Nonequilibrium Boundary-Layers," *Advances in Heat Transfer*, Academic Press, New York, 1965, p. 194.